Group-index and resonant field enhancement in a symmetric double-sided grated waveguide

Husin Alatas,[1,2,*] Hugo J. W. M. Hoekstra,[3] Alexander A. Iskandar,[1] and May-On Tjia[1]

[1]*Physics of Magnetism and Photonics Research Group, Faculty of Mathematics and Natural Sciences, Institut Teknologi Bandung, Jl. Ganesha 10, Bandung 40132, Indonesia*
[2]*Theoretical Physics Division, Department of Physics, Bogor Agricultural University, Jl. Meranti, Kampus IPB Darmaga, Bogor 16680, Indonesia*
[3]*Integrated Optical MicroSystems Group, MESA+ Research Institute for Nanotechnology, University of Twente, P.O. Box 217, 7500 AE Enschede, The Netherlands*
**Corresponding author: alatas@ipb.ac.id*

Received December 15, 2010; revised April 17, 2011; accepted April 21, 2011; posted April 26, 2011 (Doc. ID 139748); published May 24, 2011

A numerical study has been carried out by means of the Green's function method to explore possible performance improvements of a simple grated waveguide (GWg) by the variations of its grated structure. It is shown that a GWg featuring symmetric two-sided grated structure of 16 teeth with a 60 nm groove depth and having a symmetric refractive index profile with a relatively large contrast between the grated and ungrated layers is capable of delivering largely improved device performance compared to that achieved previously with a one-sided grating of 40 nm groove depth and asymmetric index profile. The improvement is characterized by a remarkable 8-fold and 15-fold increase in the group index and the maximum field intensity, respectively, at the first resonance wavelength above the upper band edge (shorter wavelength), while relatively less improvement is found at the first resonance wavelength below the lower band edge (longer wavelength). It is shown that more than 20% further improvement can be obtained by an appropriate shifting of the two innermost adjacent grating teeth in the case of the 40 nm groove depth. Apart from that, the result also reveals an interesting and remarkable correlation between the variations of the group index and the confined energy.

OCIS codes: 050.2770, 230.7400.

1. INTRODUCTION

In the studies of photonic devices in the last decade, we have witnessed rapidly growing interest in the development of slow light devices mainly for two major purposes. One is the enhancement of light-matter interaction for increased sensitivity in optical sensing. The other one is the extension of the range of group velocity variation for the operations and controls of variable optical delay lines and other photonic devices used in optical information and communication technology [1,2]. There are two main directions of development pursued by researchers for the realization of integrated optical devices for those applications. One approach adopts the basic concept of coupled resonator optical waveguides (CROWs) [3], while the other has opted for the use of photonic crystal waveguides (PhCWs) [4]. A comprehensive and direct comparison between performances of the two types of devices for communication applications has recently been reported using the same silicon-on-insulator (SOI) technological platform [5]. It was shown that both structures can be used to synchronize the orthogonally polarized data streams of a 100 Gbyte/s polarization-division multiplexing differential quadrature phase-shift keying (PolDM-DQPSK) system without corrupting the phase information. Further comparison showed that the CROW devices are preferable for operational regime of upper data rate requiring longer delays and lower loss. On the other hand, for the terabit regime, the PhCWs may offer a more favorable prospect.

The study of grated waveguides (GWgs) with quasi-two-dimensional structures has recently gained a growing interest particularly for optical sensing applications, largely due to their potential excellent performance in terms of a large group index and strongly localized field [6–14]. The planar structures considered in most of those studies also offer the benefit of greater amenability of their on-chip fabrication by the existing technology compared to the much more demanding technology for the fabrication of fully three-dimensional devices [15]. However, for a waveguide with a uniform grated section as often found in earlier studies, one has to deal with the problem of out-of-plane scattering loss arising from the mode-mismatch between the modal fields of the grated and ungrated sections. In our recent study, this issue was addressed by considering a simple model of the waveguide having a one-sided grating structure with modified edge sections using the Green's function method in the Dyson formulation [16]. It was demonstrated that an appropriately chosen symmteric tapering of the two end sections has resulted in a remarkable 85% loss reduction and 15% transmittance enhancement at the first lower (longer wavelength) band-edge resonance, with a less remarkable result found at the first upper (shorter wavelength) band-edge resonance. The enhancement of the resonance field and group index by increasing the number of grating cells as confirmed in the study, is apparently not the favorable choice as it implies an undesirable increase of the device size. Further, the same structural modifications responsible for the favorable loss reduction appeared to induce the undesirable opposite effects on the group index and field confinement. Therefore, for applications in optical sensing and time delay control (wave slowing), it is desirable

to further explore similarly simple but different GWg structures that would give rise to a significant increase in the group index as well as local field enhancement while retaining the favorable low-loss characteristic attained in the previous work [16].

In this study, we consider a GWg with double-sided grating structure and investigate the changes of the device's operational characteristics induced by a number of structural variations and different index contrasts, employing the Green's function method formulated in our previous work [16]. Presented in this are the results of investigations on structural change-induced effects on the transmittance, reflectance, scattering loss, as well as the field enhancement, group index and its slope, at both the upper and lower band-edge resonances. The results show that despite the relatively simple structural changes, it is possible to achieve truly remarkable improvements on both the group index and field enhancement over the results previously obtained with the one-sided grating structure, without seriously compromising the low-loss characteristic. The structure is further shown to offer a favorable feature for delay line application.

2. DEVICE STRUCTURE AND MATHEMATICAL FORMULATION

As shown in Fig. 1, the GWg structure considered is basically a three-layer planar-system consisting of a cover layer of refractive index n_{co}, a slab waveguide of thickness $h = 160\,\text{nm}$ and index n_{sl}, and the substrate of index n_{su}. The device features grated sections of 16 uniform teeth, both on top and beneath the slab waveguide with the groove depths of the top and bottom gratings denoted by g_t and g_b, respectively. The grating is further characterized by a periodicity of $\Lambda = 200\,\text{nm}$ and a duty cycle of 0.5, yielding a total length of $3.32\,\mu\text{m}$ for the (grating section) device. This grating structure with the exposed teeth is similar to the one investigated in a recent work [17] using the SOI technology [18,19] for better sensing performance [19]. Only the TE or *s*-polarized light (polarization along the z axis) propagating in the x direction will be considered in this study. The structure will be excited by a guided mode entering the structure from the left-hand side, employing an ungrated input feeder waveguide of the same width.

In this work, the effects of changing the structural as well as material parameters are investigated with certain ranges of variation. Our major attention is, however, focused on the effects induced by structural variations which include the case with one-sided grating ($g_b = 0$) considered previously [16] for useful comparison. The ensuing numerical study is further concentrated on the basic model of the GWg with symmetrical double-sided grating ($g_t = g_b$). A number of additional local structural variations of this model are considered for the purpose of exploring the possibility of producing further improvements on the device characteristics.

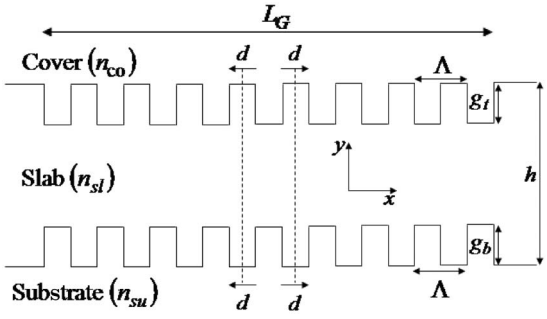

Fig. 1. Sketch of the symmetric double-sided GWg considered and the associated system parameters.

For the numerical analysis of those effects, we employ the Green's function formulation adopted in the previous study [16], because the effects of small local structural variations considered in the later part of this work can be conveniently handled by this method. For the sake of easy reference, a brief summary of the above mentioned formulation is given in the following. In this formulation, the electric field in the system is generally evaluated in terms of the associated Green's function by the following equation:

$$E_z(\boldsymbol{r}) = E_z^B(\boldsymbol{r}) + \int_A G(\boldsymbol{r},\boldsymbol{r}')k_0^2\Delta\varepsilon(\boldsymbol{r}')E_z^B(\boldsymbol{r}')\mathrm{d}\boldsymbol{r}', \tag{1}$$

with the Green's function G given by

$$G(\boldsymbol{r},\boldsymbol{r}') = G^B(\boldsymbol{r},\boldsymbol{r}') + \int_A G^B(\boldsymbol{r},\boldsymbol{r}'')k_0^2\Delta\varepsilon(\boldsymbol{r}'')G(\boldsymbol{r}'',\boldsymbol{r}')\mathrm{d}A'', \tag{2}$$

where E_z^B is the background field of the fundamental TE mode of the ungrated slab waveguide of thickness 160 nm, and G^B is the background Green's function of the ungrated three-layer system. Note further that $(\boldsymbol{r},\boldsymbol{r}') = (x,y,x',y')$, $k_0 = \omega/c$ which is the free-space wave number, $\Delta\varepsilon = \varepsilon - \varepsilon_B$ which is the contrast between the permittivities of the scatterer (ε) and the background (ε_B), while A is the area of integration covering the entire computational domain. The complete and detailed expressions of G^B in terms of its Fourier components for each layer in this structure were derived in [16] following the method formulated in previous works [20–22]. It is worth noting that this method implicitly includes a built-in perfectly transparent boundary, and hence a relatively small computational window is sufficient to produce reliable computational results. We have accordingly defined the computational window in this study by $[x_l, x_r] = [0, 8]\,\mu\text{m}$ and $[y_l, y_u] = [-0.04, 0.2]\,\mu\text{m}$, with the corresponding meshes are chosen to be $\Delta x = 10\,\text{nm}$ and $\Delta y = 20\,\text{nm}$. It is also important to note that the system considered is assumed to be intrinsically lossless.

The transmittance (T), reflectance (R), and loss per unit length (L) parameters of the device are calculated on the basis of the following definitions:

$$T = \frac{\int_0^h |E_z(x_t,y;\lambda)|^2\mathrm{d}y}{\int_0^h |E_{z,0}(x_i,y;\lambda)|^2\mathrm{d}y}, \tag{3}$$

$$R = \frac{\int_0^h |E_z(x_i,y;\lambda) - E_{z,0}(x_i,y;\lambda)|^2\mathrm{d}y}{\int_0^h |E_{z,0}(x_i,y;\lambda)|^2\mathrm{d}y}, \tag{4}$$

$$L = \frac{1 - T - R}{L_G}, \tag{5}$$

respectively, where $L_G = 3.32\,\mu\text{m}$ is the total length of the grated section, while x_i and x_t denote the positions located at $0.5\,\mu\text{m}$ from the left and right grating ends, respectively, which are far enough to eliminate the effects of scattered

fields. Further, $E_z(x_i, y; \lambda)$ and $E_z(x_t, y; \lambda)$ are the fields at x_i and x_t, respectively, while $E_{z,0}(x_i, y; \lambda)$ is the guided fundamental modal field at x_i.

The other two additional parameters to be investigated are the group index (N_g) and the quality of energy confinement (W). The group index is calculated according to the following definitions, respectively, [23]:

$$N_g = \frac{c\tau_g}{L_G} = -\frac{\lambda^2 d\phi/d\lambda}{2\pi L_G}, \tag{6}$$

where τ_g is the group-delay of the resonator, while ϕ is the phase of the following complex transmission coefficient:

$$t = \frac{\int_0^h E_z(x_R, y; \lambda)\mathrm{d}y}{\int_0^h E_{z,0}(x_L, y; \lambda)\mathrm{d}y}. \tag{7}$$

Here, x_L and x_R denote the positions of the left and right grating ends, respectively. It is clear from the definition of the group index (6) that the time-delay slope is defined as follows:

$$\frac{d\tau_g}{d\lambda} = \frac{L_G}{c}\frac{dN_g}{d\lambda}. \tag{8}$$

Note that the time-delay slope (8) is proportional to the group-index slope $dN_g/d\lambda$. For the calculation of the energy W confined within a certain area A, we adopt the following definition:

$$W = \int_A \varepsilon_{\mathrm{slab}}|E|^2\mathrm{d}A, \tag{9}$$

where A covers the ungrated waveguide area in the grated section.

3. RESULTS AND DISCUSSIONS

A. Effects of Increasing Refractive Index Contrast

Let us first consider the case having one-sided grating with $n_{\mathrm{co}} = 1.98$, $n_{\mathrm{sl}} = 3.48$, $n_{\mathrm{su}} = 1.98$, $g_t = 40\,\mathrm{nm}$, and $g_b = 0\,\mathrm{nm}$. The upper and lower resonance wavelengths are given in this case by $\lambda^u_{\mathrm{res}} = 1073\,\mathrm{nm}$ and $\lambda^l_{\mathrm{res}} = 1187\,\mathrm{nm}$, respectively. For the upper resonance, we find $T = -0.146\,\mathrm{dB}$, $R = -29.59\,\mathrm{dB}$ and $L = -4.503\,\mathrm{dB}/\mu\mathrm{m}$, $N_g = 4.007$, $dN_g/d\lambda = 0.029\,\mathrm{nm}^{-1}$, $|E_{\max}|^2 = 4.339\,(\mathrm{a.u.})$, and $W = 5.132\,(\mathrm{a.u.})$, while for the lower resonance the calculated result gives $T = -0.078\,\mathrm{dB}$, $R = -36.38\,\mathrm{dB}$ and $L = -5.280\,\mathrm{dB}/\mu\mathrm{m}$, $N_g = 3.941$, $dN_g/d\lambda = -0.026\,\mathrm{nm}^{-1}$, $|E_{\max}|^2 = 4.150\,(\mathrm{a.u.})$, and $W = 5.160\,(\mathrm{a.u.})$. This is to be compared with the result for the same geometrical structure, but with a refractive index profile specified by $n_{\mathrm{co}} = 1$, $n_{\mathrm{sl}} = 1.98$, $n_{\mathrm{su}} = 1.44$, calculated previously for x_i and x_t at 1 and 3 μm from the left and right ends of the grating, respectively, in order to avoid the more extended scattered fields [16]. It was found for this case that: $T = -0.177\,\mathrm{dB}$, $R = -30.22\,\mathrm{dB}$, $L = -4.247\,\mathrm{dB}/\mu\mathrm{m}$, $N_g = 2.092$, $dN_g/d\lambda = 0.008\,\mathrm{nm}^{-1}$, $|E_{\max}|^2 = 3.318\,(\mathrm{a.u.})$, and $W = 2.931\,(\mathrm{a.u.})$ at the upper resonance wavelength of $\lambda^u_{\mathrm{res}} = 627\,\mathrm{nm}$. On the other hand, for the lower resonance at $\lambda^l_{\mathrm{res}} = 693\,\mathrm{nm}$, the calculated result for the parameters are given by $T = -0.082\,\mathrm{dB}$, $R = -40.46\,\mathrm{dB}$, $L = -5.220\,\mathrm{dB}/\mu\mathrm{m}$, $N_g = 2.029$, $dN_g/d\lambda = -0.010\,\mathrm{nm}^{-1}$, $|E_{\max}|^2 = 3.107\,(\mathrm{a.u.})$, and $W = 2.919\,(\mathrm{a.u.})$. Compared with the present case of the symmetric index profile, the previous structure exhibits more asymmetric transmission characteristics and relatively higher losses, as well as less confined energy and upper group indices at both upper and lower resonances. Thus, we have shown that an overall improvement is achieved with a larger index contrast, with the group index acquiring the most pronounced enhancement marked by roughly twofold increases at both resonances.

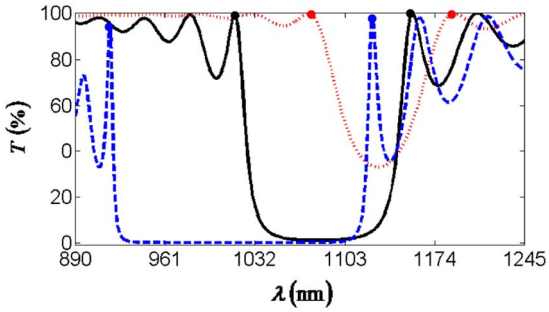

Fig. 2. (Color online) Transmittance T for the cases with groove depths $g_t = g_b = 20\,\mathrm{nm}$ (red dotted curve), 40 nm (black solid curve), and 60 nm (blue dashed curve).

B. Further Improvements with the Double-Sided Grating Structure

Next, we consider structural variation from the case of symmetric index profiles with one-sided grating to the case with symmetric double-sided grating structures of three different groove depths namely $g_t = g_b = 20$, 40, and 60 nm. Presented in Fig. 2 are the transmittance (T) spectra of those three different structures with the upper and lower first resonance wavelengths given respectively by $\lambda^u_{\mathrm{res}} = 1075$, 1016, 917.6 nm and $\lambda^l_{\mathrm{res}} = 1189$, 1156, 1124.6 nm for each of the three cases

Table 1. Calculated Operational Parameters of the Symmetric ($g_t = g_b$) Double-Sided GWg for Different Groove Depths at the Upper Resonance and Lower Resonance, Showing the Most Favorable Improvement Attained with a 60 nm Groove Depth

Upper Resonance								
g_t, g_b (nm)	λ^u_{res} (nm)	T (dB)	R (dB)	L (dB/μm)	N_g	$dN_g/d\lambda$ (nm^{-1})	$\lvert E_{\max}\rvert^2$ (a.u.)	W (a.u.)
20	1074	~0	−51.56	−23.06	3.970	0.031	4.68	12.17
40	1016	−0.002	−43.98	−10.05	6.501	0.275	14.14	15.57
60	917.6	−0.252	−36.99	−3.765	16.68	1.975	52.66	23.95
Lower Resonance								
g_t, g_b (nm)	λ^l_{res} (nm)	T (dB)	R (dB)	L (dB/μm)	N_g	$dN_g/d\lambda$ (nm^{-1})	$\lvert E_{\max}\rvert^2$ (a.u.)	W (a.u.)
20	1189	~0	−44.06	−18.48	3.950	−0.024	4.29	12.10
40	1156	−0.001	−35.53	−14.15	6.693	−0.207	11.56	14.00
60	1124.6	−0.079	−36.58	−5.265	15.20	−1.225	33.26	15.79

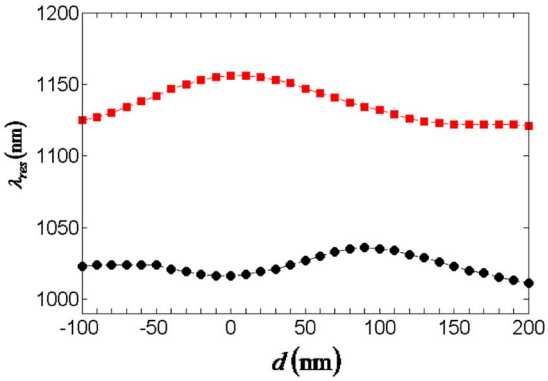

Fig. 3. (Color online) Left (black solid circle) and lower (red solid square) resonance wavelenghts for $g_t = g_b = 40$ nm.

of different groove depths, as displayed in the figure. It is seen that the resonance wavelengths are consistently shifted to the smaller values (blue shifted) with an increasing groove depth. The most remarkable is the effect on the gap characteristics, which exhibit the changes toward deeper and broader gaps as the groove depth is increased, indicating the increased influence of the grating structure.

Further, the calculated results of the operational parameters are summarized in Table 1 for the upper and lower resonances. It is observed that except for the case with the shallowest grooves, which feature closely equivalent operational characteristics at the two resonance wavelengths, the other two cases of larger groove depths generally possess perceptibly different characteristics at the two edge resonances. Most remarkable are the monotonous and considerable increase of N_g, $|E_{\max}|^2$, and W with increasing groove depth at both the upper and lower resonances, yielding the largest value of $N_g = 16.68$, $|E_{\max}|^2 = 52.66$ (a.u.), and $W = 23.95$ (a.u.) at the upper resonance for groove depth 60 nm. Although this is achieved at the expense of a concurrent and monotonous increase of the loss, even the largest loss of -3.765 dB/μm found for the case of the 60 nm groove depth at $\lambda^u_{\text{res}} = 917.6$ nm to be still a relatively insignificant increase compared with the value $L = -4.247$ dB/μm attained in the case of one-sided GWg cited earlier. This is indeed a small price that one has to pay compared with the great benefit gained from the very large increases in those three important parameters. Compared with the result obtained in the previous case of a one-sided grating with an asymmetric refractive index profile and a 40 nm groove depth, the increases marked by more than 15-folds for $|E_{\max}|^2$ and more than 8-folds for N_g and W. It is important to add that along with the largest group index of the device, $N_g = 16.68$ attained at the upper resonance also offers the corresponding group index slope of $dN_g/d\lambda = 1.975\,\text{nm}^{-1}$ which amounts to a time-delay slope of 0.022 ps/nm for the total length of $L_G = 3.32\,\mu$m. This is to be compared with the performance characterized by a time-delay slope 6 ps/nm as reported previously for a 4 mm PhCW operated at the third telecom window [5]. The comparison clearly suggests the possibility of achieving the desirable performance with further device miniaturization.

C. Effects of Further Structural Modifications

The following study is focused on the effects of the basic patterns of performance variations affected by shifting the

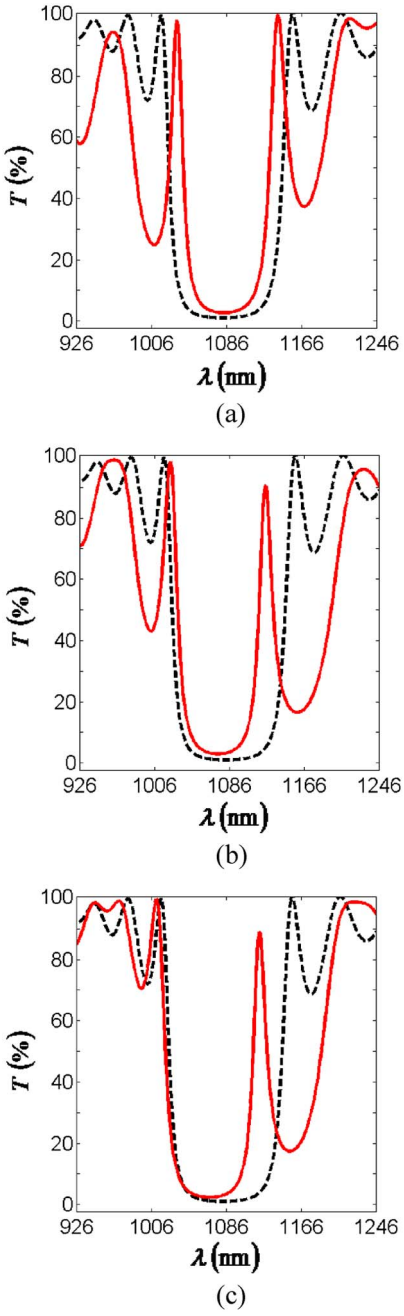

Fig. 4. (Color online) Transmittance (T) (red solid curve) for $g_t = g_b = 40$ nm and (a) $d = 70$ nm, (b) $d = -100$ nm, and (c) $d = 200$ nm, along with T for $d = 0$ nm (black dashed curve).

two adjacent middle teeth for various distances denoted by the shift parameter d, denoted in Fig. 1, with $d > 0$ and $d < 0$ referring to the outward and inward shifts, respectively. For this study, the case of a 40 nm instead of a 60 nm groove depth has been chosen for the study of detailed effects mentioned above as the former is less demanding on the computational labor and time. Note that for $d = 200$ nm, each of the teeth ends up merging fully with its outer neighboring tooth, leaving a 500 nm wide groove in the middle of the newly formed GWg. On the other hand, for $d = -100$ nm, both teeth merge fully into a single tooth in the middle of the new structure, separated from the adjacent tooth on each side with a grooves width of 200 nm.

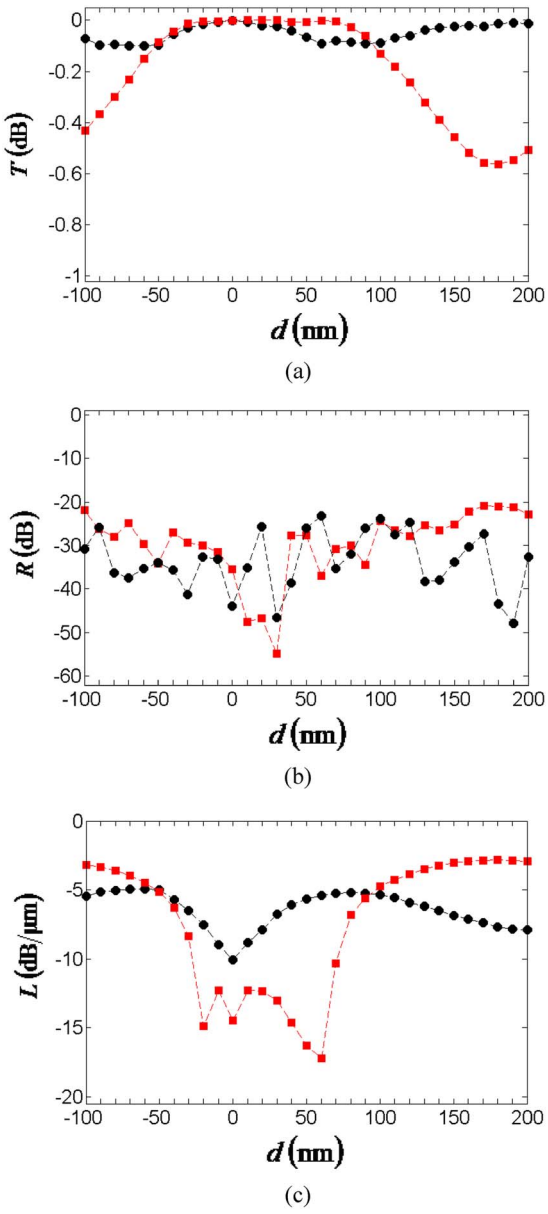

Fig. 5. (Color online) Variations of the (a) the transmittance (T), (b) reflectance (R), and (c) loss per unit length (L) with respect to d at the upper (black solid circle) and lower (red solid square) resonances.

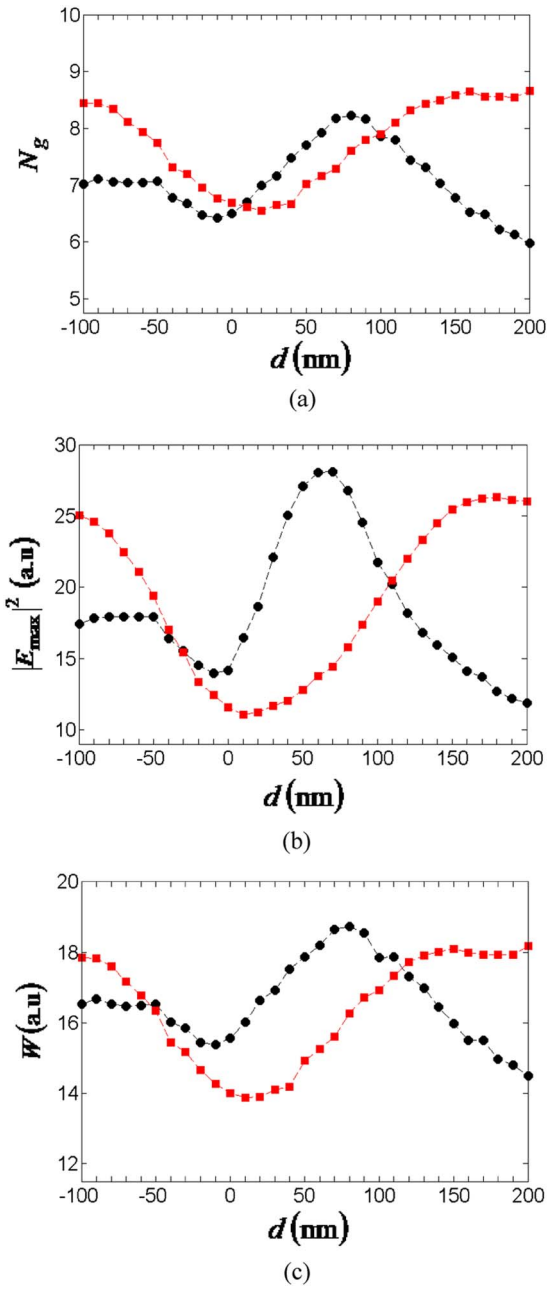

Fig. 6. (Color online) Variations of the parameters (a) N_g, (b) $|E_{\max}|^2$, and (c) W with respect to d at the upper (black solid circle) and lower (red solid square) resonances.

Similar to the g dependence of $\lambda^u_{\rm res}$ and $\lambda^l_{\rm res}$ exhibited in the unshifted case ($d = 0$ nm), the resonance wavelengths are also found to vary with d, as shown in Fig. 3 for the variation of d over the range $d = -100$ to 200 nm. It is seen that both $\lambda^u_{\rm res}$ and $\lambda^l_{\rm res}$ appear to vary nonmonotonously in opposite trends, and their difference tends to decrease at $d = -100$ nm and $d = 200$ nm. Depicted in Figs. 4(a)–4(c) are the transmission characteristics for the cases of $d = 70$ nm, $d = -100$ nm, and $d = 200$ nm, respectively. Compared to the case of $d = 0$ nm represented by the dashed spectrum, an outward shift with $d = 70$ nm is found to move both resonance wavelengths toward the gap center, resulting in a narrower gap with a slight decrease in T at the upper resonance. On the other hand, for cases with $d = -100$ nm and $d = 200$ nm, only the lower resonance wavelengths are seen to move further toward the gap center with each associated transmittance showing a perceptible decrease. Meanwhile, the upper resonance in each case appears to move back toward its original position by the same amount of shifts in the corresponding $\lambda^l_{\rm res}$, leaving the gap width roughly unchanged.

The detailed variations of the transmittance (T), reflectance (R), and loss per unit length (L) as well as N_g, $|E_{\max}|^2$, and W as functions of d are given in Figs. 5 and 6, respectively. All of them show nonmonotonous and generally different, and mostly opposite variations with respect to d, leading to the appearance of intersecting points indicated in the Figures. The only exception is the behavior of R which remains low over the entire range of d at both resonance wavelengths. Further, the effects on the spatial intensity distribution related

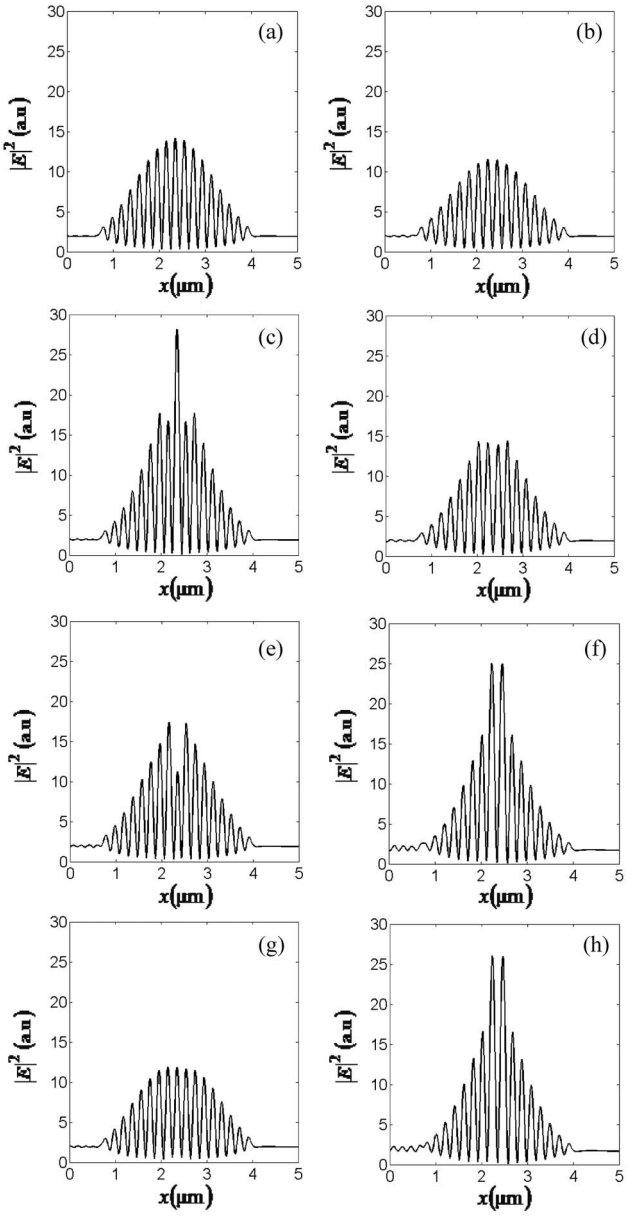

Fig. 7. Spatial distribution of $|E|^2$ along the x axis at $z = 0.08\,\mu$m at the upper resonance (left panel) for (a) $d = 0$ nm, (c) $d = 70$ nm, (e) $d = -100$ nm, and (g) $d = 200$ nm, with (b), (d), (f), and (h) present the distributions for the same series of d's at lower resonance (right panel).

with the confined energy W are described in Figs. 7. The result presented in Fig. 7(c) shows the highest maximum intensity at $\lambda^u_{\mathrm{res}} = 1033$ nm for $d = 70$ nm, featuring a 1.988 fold enhancement with respect to $|E_{\max}|^2$ of the unshifted case. The intensity distribution depicted in the figure exhibits a very sharp profile at the center of the GWg, indicating the presence of a defect mode characterized by an exponential decay (localization) of the field as indicated by the intensity profile mentioned above. For this particular case, the enhancement factors for N_g and W with respect to the unshifted case are 1.257 and 1.198, respectively, amounting to roughly 20% enhancement. Although these favorable improvements are accompanied by an increase of the loss from $L = -10.05$ dB/μm to $L = -5.241$ dB/μm, it is still slightly less than the best figure ($L = -5.220$ dB/μm) obtained previously with the one-sided

Table 2. Further Variations of the Operational Parameters as the Results of Shifting the Two Adjacent Middle Teeth by Different Distances for the Upper and Lower Resonances

Upper Resonances						
d (nm)	λ^u_{res} (nm)	L (dB/μm)	N_g	$dN_g/d\lambda$ (nm^{-1})	$\lvert E_{\max}\rvert^2$ (a.u.)	W (a.u.)
0	1016	−10.05	6.501	0.275	14.14	15.57
70	1033	−5.223	8.173	0.200	28.11	18.66
−100	1023	−5.446	7.023	0.161	17.40	16.53
200	1011	−7.913	5.975	0.223	11.87	14.50
Lower Resonances						
d (nm)	λ^l_{res} (nm)	L (dB/μm)	N_g	$dN_g/d\lambda$ (nm^{-1})	$\lvert E_{\max}\rvert^2$ (a.u.)	W (a.u.)
0	1156	−14.15	6.693	−0.207	11.56	14.00
70	1141	−10.30	7.286	−0.199	14.40	15.60
−100	1125	−3.172	8.449	−0.226	23.03	17.85
200	1121	−2.949	8.625	−0.182	26.03	18.18

GWg [16]. The intensity profile shown in Fig. 7(d) for the same case at $\lambda^l_{\mathrm{res}} = 1141$ nm is clearly devoid of the same exponential intensity profile and yields even smaller enhancement factors of N_g, $|E_{\max}|^2$, and W of 1.089, 1.246, and 1.114, respectively, but a remarkably smaller loss of $L = -10.30$ dB/μm. It is interesting to note, however, that the intensity profiles shown in Figs. 7(c) and 7(d) for $d = 70$ nm display roughly an opposite pattern of contrast compared to those presented in Figs. 7(e) and 7(f) for $d = -100$ nm, although the corresponding pairs [Figs. 7(d) and 7(e) and Figs. 7(c) and 7(f)] do appear to differ from each other in some peculiar details.

The effects of different d's on all the pertinent operational parameters at both resonances are summarized in Table 2. Apparently, no general pattern of variation has emerged from the calculated variations of the operational parameters due to systematic changes of the shift parameter d. In other words, a trade-off among those parameters must be considered for each specific application. In spite of that, we have been tempted to look into the possible relation between the detailed variations of N_g and W given in Figs. 6. The results plotted in Fig. 8 do reveal an interesting, nearly linear correlation which is worthy of further study.

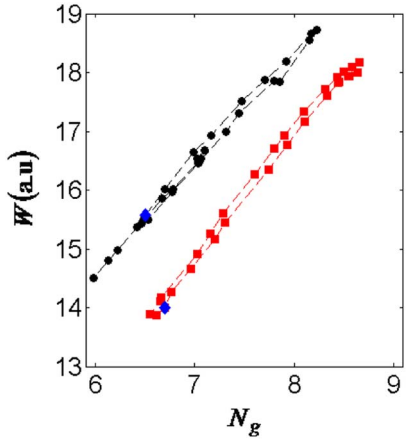

Fig. 8. (Color online) Correlation between the variations of N_g and W deduced from the calculated results at the upper (black solid circle) and lower (red solid square) resonances as presented in Fig. 6. The blue solid diamond denotes the (N_g, W) of an unshifted structure.

4. SUMMARY

Employing the Green's function method, this numerical study has demonstrated the possibility of achieving high performance GWg with a double-sided grated structure and proper choice of the material indices as well as the structural parameters. It is shown that a symmetric two-sided GWg with a slab thickness of 160 nm and uniform groove depth of 60 nm may deliver the best performances marked by $N_g = 16.68$, $dN_g/d\lambda = 1.975\,\mathrm{nm}^{-1}$, $|E_{\max}|^2 = 52.66\,(\mathrm{a.u.})$, $W = 23.95\,(\mathrm{a.u.})$, and $L = -3.765\,\mathrm{dB}/\mu\mathrm{m}$ at $\lambda_{\mathrm{res}}^{u} = 917.6\,\mathrm{nm}$ and $N_g = 15.20$, $dN_g/d\lambda = -1.225\,\mathrm{nm}^{-1}$, $|E_{\max}|^2 = 33.26\,(\mathrm{a.u.})$, $W = 15.79$ (a.u.), and $L = -5.265\,\mathrm{dB}/\mu\mathrm{m}$ at $\lambda_{\mathrm{res}}^{l} = 1124.6\,\mathrm{nm}$. Further improvements of more than 20% in N_g, $|E_{\max}|^2$, and W can also be achieved by an appropriate shift of the two innermost adjacent teeth of the gratings. In addition to that, the detailed variations of N_g and W are shown to exhibit an unexpected and interesting near linear correlation.

ACKNOWLEDGMENTS

This work is supported by the Royal Netherlands Academy of Arts and Sciences (KNAW) through the Scientific Programme Indonesia-Netherlands, project ref. 07-PD-12.

REFERENCES

1. R. S. Tucker, P. C. Ku, and C. J. Chang-Hasnain, "Slow-light optical buffers: capabilities and fundamental limitations," J. Lightwave Technol. **23**, 4046–4066 (2005).
2. M. Zhang, N. Groothoff, A. C. Krüger, P. Shi, and M. Kristensen, "Direct slow-light excitation in photonic crystal waveguides forming ultra-compact splitters," Opt. Express **19**, 7120–7126 (2011).
3. J. Goeckeritz and S. Blair, "Optical characterization of coupled resonator slow-light rib waveguides," Opt. Express **18**, 18190–18199 (2010).
4. J. Li, T. P. White, L. O'Faolain, A. Gomez-Iglesias, and T. F. Krauss, "Systematic design of flat band slow light in photonic crystal waveguides," Opt. Express **16**, 6227–6232 (2008).
5. A. Melloni, A. Canciamilla, C. Ferrari, F. Morichetti, L. O'Faolain, T. F. Krauss, R. De La Rue, A. Samarelli, and M. Sorel, "Tunable delay lines in silicon photonics: coupled resonators and photonic crystals a comparison," IEEE Photonics J. **2**, 181–194 (2010).
6. O. M. Mendez and J. S. Martinez, "Scattering of TE-polarized waves by a finite grating: giant resonant enhancement of the electric field within the grooves," J. Opt. Soc. Am. A **14**, 2203–2211 (1997).
7. T. C. Kleckner, D. Modotto, A. Locatelli, J. P. Mondia, S. Linden, R. Morandotti, C. De Angelis, C. R. Stanley, H. M. Van Driel, and J. S. Aitchison, "Design, fabrication, and characterization of deep-etched waveguide gratings," J. Lightwave Technol. **23**, 3832–3842 (2005).
8. W. C. L. Hopman, P. Pottier, D. Yudistira, J. Van Lith, P. V. Lambeck, R. M. De La Rue, A. Driessen, H. J. W. M. Hoekstra, and R. M. de Ridder, "Quasi-one-dimensional photonic crystal as a compact buiding block for refractometric optical sensors," IEEE J. Sel. Top. Quantum Electron. **11**, 11–16 (2005).
9. W. C. L. Hopman, R. Dekker, D. Yudistira, W. F. A. Engbers, H. J. W. M. Hoekstra, and R. M. de Ridder, "Fabrication and characterization of high-quality uniform and apodized Si3N4 waveguide gratings using laser interference lithography," IEEE Photon. Technol. Lett. **18**, 1855–1857 (2006).
10. W. C. L. Hopman, H. J. W. M. Hoekstra, R. Dekker, L. Zhuang, and R. M. de Ridder, "Far-field scattering microscopy applied to analysis of slow light, power enhancement, and delay times in uniform Bragg waveguide gratings," Opt. Express **15**, 1851–1870 (2007).
11. J.-W. Mu, H. Zhang, and W.-P. Huang, "Design of waveguide Bragg gratings with strong index corrugations," J. Lightwave Technol. **26**, 1596–1601 (2008).
12. F. Riboli, P. Bettotti, and L. Pavesi, "Band gap characterization and slow light effects in one dimensional photonic crystals based on silicon slot-waveguides," Opt. Express **15**, 11769–11775 (2007).
13. M. L. Povinelli, Steven G. Johnson, and J. D. Joannopoulos, "Slow-light, band-edge waveguides for tunable time delays," Opt. Express **13**, 7145–7159 (2005).
14. C. Wei, S. Liu, D. Deng, J. Shen, J. Shao, and Z. Fan, "Electric field enhancement in guided-mode resonance filters," Opt. Lett. **31**, 1223–1225 (2006).
15. S. Noda, "Recent progresses and future prospects of two and three-dimensional photonic crystals," J. Lightwave Technol. **24**, 4554–4567 (2006).
16. H. Alatas, A. A. Iskandar, H. J. W. M. Hoekstra, and M. O. Tjia, "Performance changes of a grated waveguide at resonance wavelengths next to its band-edges due to modified edge sections," J. Opt. Soc. Am. B **27**, 2743–2749 (2010).
17. M. Gnan, W. C. L. Hopman, G. Bellanca, R. M. De Ridder, R. M. De La Rue, and P. Bassi, "Closure of the stop-band in photonic wire Bragg gratings," Opt. Express **17**, 8830–8842 (2009).
18. M. Gnan, G. Bellanca, H. Chong, P. Bassi, and R. M. De La Rue, "Modelling of photonic wire Bragg gratings," Opt. Quantum. Electron. **38**, 133–148 (2006).
19. A. S. Jugessur, J. Ou, S. Aitchison, R. M. De La Rue, and M. Gnan, "A photonic nano-Bragg grating device integrated with microfluidic channels for bio-sensing applications," Microelectron. Eng. **86**, 1488–1490 (2009).
20. M. Paulus and O. J. F. Martin, "Green's tensor technique for scattering in two dimensional stratified media," Phys. Rev. E **63**, 066615 (2001).
21. M. Paulus, P. Gay-Balmaz, and O. J. F. Martin, "Accurate and efficient computation of Green's tensor for stratified media," Phys. Rev. E **62**, 5797–5809 (2000).
22. O. J. F. Martin and N. B. Piller, "Electromagnetic scattering in polarizable backgrounds," Phys. Rev. E **58**, 3909–3915 (1998).
23. J. M. Bendickson, J. P. Dowling, and M. Scalora, "Analytic expressions for the electromagnetic mode density in finite, one-dimensional, photonic band-gap structures," Phys. Rev. E **53**, 4107–4121 (1996).